Chapter 2
6-DOF Shaker Test Input Derivation from Field Test

Michael Ross, Laura D. Jacobs, Greg Tipton, Garrett Nelson, Kevin Cross, Norman Hunter, and Julie Harvie

Abstract Six degree of freedom (6-DOF) subsystem/component testing is becoming a desirable method, for field test data and the stress environment can be better replicated with this technology. Unfortunately, it is a rare occasion where a field test can be sufficiently instrumented such that the subsystem/component 6-DOF inputs can be directly derived. However, a recent field test of a Sandia National Laboratory system was instrumented sufficiently such that the input could be directly derived for a particular subsystem. This input is compared to methods for deriving 6-DOF test inputs from field data with limited instrumentation. There are four methods in this study used for deriving 6-DOF input with limited instrumentation. In addition to input comparisons, response measurements during the flight are compared to the predicted response of each input derivation method. All these methods with limited instrumentation suffer from the need to inverse the transmissibility function.

Keywords Multi-input multi-output (MIMO) • 6-DOF vibration • Multi-axis vibration • Environmental test specification • Input derivation

2.1 Introduction

During typical field tests of systems, it is rare to have sufficient instrumentation to measure or derive the six degree of freedom (6-DOF) inputs to either a subsystem or component. These tests are designed to subject an instrumented system to environments such as transportation, handling, and flight as would be seen in its final operating environment. Subsequently, the results of these tests can be used to gain an understanding of the system's behavior during these environments. Multi-axis vibration testing is gaining popularity as a method to simulate these environmental conditions in a lab setting. It has been shown that when compared to other lab test methods, full 6-DOF testing produces a more realistic stress state in the subsystem or component [1].

A key element to the successful simulation of a field environment with multi-axis shaker systems in the laboratory is the input specification which is used to define the desired dynamics of the test. This paper explores four different methods of deriving these inputs for a 6-DOF shaker system given the absence of a direct measurement of the 6-DOF inputs in field data. Each method requires the development of a transmissibility function, which will need to be inverted during the derivation process. In addition to numerical errors caused by this inversion, there may be additional errors encountered due to the use of a different unit in the field and laboratory tests, as well as a change in boundary conditions between the two test environments. By construct, the different derivation methods try to match responses at key locations during the laboratory test to those in the field. Accordingly, the inverse methodologies which were implemented may potentially correct some of these errors.

An accompanying paper discusses the experimental set-up and results of the laboratory tests conducted [2]. Given that the ultimate goal of these tests is to recreate the field environment, the response of the system in the lab is compared to that measured in the field. A close agreement between these two datasets is used as an indication of the performance of each specification derivation method explored. This paper uses the transmissibility function and the derived inputs obtained from each method to make predictions of the dynamic responses of the system under investigation. Subsequently, these responses are compared to those originally obtained in the field. Each method was explored for two distinct test cases: (1) a full 6-DOF input consisting of three translations and three rotations and (2) a 3-DOF input of consisting of only the translations. In the

M. Ross (✉) • L.D. Jacobs • G. Tipton • G. Nelson • K. Cross • N. Hunter
Sandia National Laboratories, P.O. Box 5800, Albuquerque, NM 87185, USA
e-mail: mross@sandia.gov

J. Harvie
Environments Engineering and Integration Department, Sandia National Laboratories, P.O. Box 5800-MS 0840, Albuquerque, NM 87185, USA

J.M. Harvie, J. Baqersad (eds.), *Shock & Vibration, Aircraft/Aerospace, Energy Harvesting, Acoustics & Optics, Volume 9*,
Conference Proceedings of the Society for Experimental Mechanics Series, DOI 10.1007/978-3-319-54735-0_2

results presented, it will be shown that the 3-DOF input under-drives the responses, the Smallwood–Cap method [3] produces the least amount of predicted error, and that scaling has very little effect on the error. The fact that the scaling has little effect on the error is important, because it has been shown that the input spectral density matrix may not be positive semidefinite, and scaling will correct this problem [4].

2.1.1 Overall Concept

Ultimately, in this work, it is desirable to reproduce the response of a system's internal dynamics (as measured at key positions with an accelerometer) during a single field test in the laboratory with the use of 6-DOF shaker table. The following process was used as the framework for this investigation:

1. Provide an estimated flight level input to the system on the 6-DOF shaker table. Using the responses measured to this input, derive a transmissibility function, $\boldsymbol{H}(\omega)$, from the input to the response locations. The details of this step are discussed in Sect. 2.2.
2. Using actual flight test responses and the transmissibility function, $\boldsymbol{H}(\omega)$, develop a set of inputs, $\boldsymbol{S}_{xx}(\omega)$, in terms of the power spectral density matrix that will, as best as possible, replicate internal response from flight if used as input for the 6-DOF shaker table. This is discussed in Sect. 2.3.
3. Perform a forward problem to predict the responses in the lab using the transmissibility functions and the calculated inputs and compare those to the flight data. This comparison is discussed in Sect. 2.4.
4. Perform the 6-DOF shaker test with these inputs and compare the results to actual flight test data. The laboratory results will be discussed in the companion paper [2].

2.2 Deriving the Transmissibility Function

When deriving the transmissibility function from both the input and output responses of the system on a 6-DOF shaker, a mathematical model is constructed. The model derived from this experimental data is known as an experimentally derived model (EDM), $\boldsymbol{H}(\omega)_{EDM}$. For the remainder of this paper, the subscript EDM is assumed on all transmissibility matrices. A bold variable is used to represent either a matrix or a vector. Like all mathematical models, the EDM has certain limitations and assumptions. One assumption is that the system will remain linear. In an effort to reduce the error associated with the linear assumption, it is best to derive the transmissibility function with inputs as close to the environment that is being replicated as possible.

As previously mentioned, all methods used in this work require the use of a transmissibility function. Typically, this frequency dependent function is defined in a simple input/output system as

$$\boldsymbol{Y}(\omega) = \boldsymbol{H}'_{\boldsymbol{xy}}(\omega)\,\boldsymbol{X}(\omega)\,, \tag{2.1}$$

where $\boldsymbol{Y}(\omega)$ is a column vector representing the Fourier transforms of the output responses, $\boldsymbol{H}(\omega)$ is the transmissibility matrix, and $\boldsymbol{X}(\omega)$ is a column vector representing the Fourier transform of the inputs. When using random vibration data, the transmissibility matrix can be found using the following form [5].

$$\boldsymbol{H}_{\boldsymbol{xy}}(\omega) = \boldsymbol{G}_{\boldsymbol{xx}}^{-\dagger}(\omega)\,\boldsymbol{G}_{\boldsymbol{xy}}(\omega)\,, \tag{2.2}$$

where $\boldsymbol{G}_{xx}(\omega)$ is the input spectral density matrix, $\boldsymbol{G}_{xy}(\omega)$ is the input/ouput cross-spectral density matrix, and the superscript $[\,]^{-\dagger}$ represents the Moore-Penrose generalized inverse of the matrix. Equation (2.2) requires an input autospectral density matrix that is found from three translational accelerations $(\ddot{x}, \ddot{y}, \ddot{z})$, and three rotational accelerations$(r\ddot{x}, r\ddot{y}, r\ddot{z})$. The method to determine these six inputs is discussed next.

It has been found that these six inputs can best be replicated by using a set of tri-axial accelerometers located at the corners of the fixture [6], as seen in Fig. 2.1, and referred to as the fixture gages. The six inputs are found at a virtual location by assuming the fixture remains rigid in the frequencies of interest.

The input at the virtual location is found using an inverse method given the responses of the fixture gages. The forward problem is written as seen in Eq. (2.3).

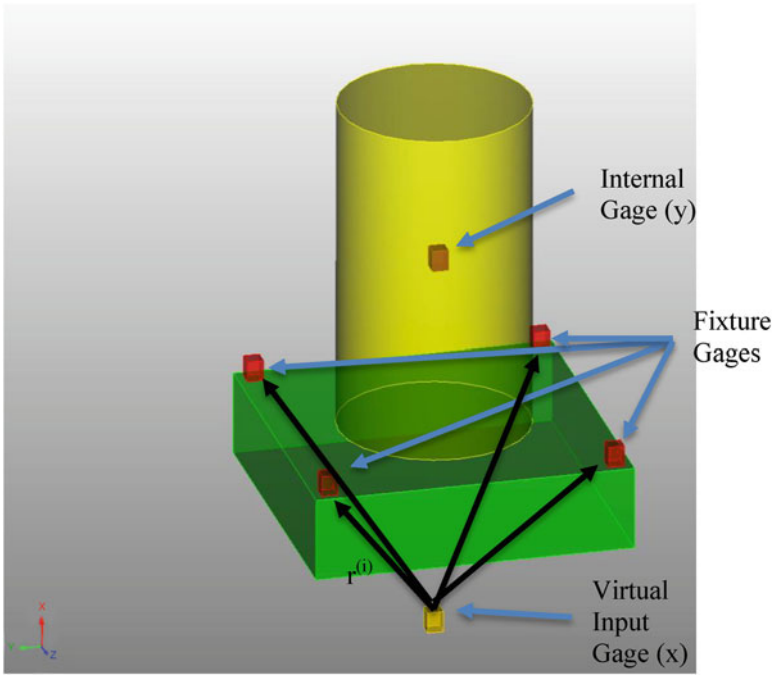

Fig. 2.1 Experimental set-up with fixture gages and a virtual input gage used to derive the transmissibility function

$$\begin{Bmatrix} \ddot{x}_1 \\ \ddot{y}_1 \\ \ddot{z}_1 \\ \vdots \\ \ddot{x}_4 \end{Bmatrix}_{12x1} = \begin{bmatrix} 1\,0\,0 & 0 & r_z^1 & -r_y^1 \\ 0\,1\,0 & -r_z^1 & 0 & r_x^1 \\ 0\,0\,1 & r_y^1 & -r_x^1 & 0 \\ 1\,0\,0 & 0 & r_z^2 & -r_y^2 \\ 0\,1\,0 & -r_z^2 & 0 & r_x^2 \\ 0\,0\,1 & r_y^2 & -r_x^2 & 0 \\ 1\,0\,0 & 0 & r_z^3 & -r_y^3 \\ 0\,1\,0 & -r_z^3 & 0 & r_x^3 \\ 0\,0\,1 & r_y^3 & -r_x^3 & 0 \\ 1\,0\,0 & 0 & r_z^4 & -r_y^4 \\ 0\,1\,0 & -r_z^4 & 0 & r_x^4 \\ 0\,0\,1 & r_y^4 & -r_x^4 & 0 \end{bmatrix} \begin{Bmatrix} \ddot{x} \\ \ddot{y} \\ \ddot{z} \\ r\ddot{x} \\ r\ddot{y} \\ r\ddot{z} \end{Bmatrix}_{6x1} \tag{2.3}$$

Equation (2.3) can be written in compact form as

$$\boldsymbol{a_f} = \boldsymbol{R}\boldsymbol{a}_x, \tag{2.4}$$

where $\boldsymbol{a_f}$ contains the fixture gage responses, $\boldsymbol{R}$ is a geometric relation matrix with r being the moment arm from the virtual location to the fixture gage, and $\boldsymbol{a}_x$ contains the desired translational and rotational inputs to the system. A least squares solution is found for $\boldsymbol{a}_x = \boldsymbol{R}^{-1}\boldsymbol{a}_f$. The virtual input accelerations and rotations in conjunction with internal responses are then used to find $\boldsymbol{G}_{xx}(\omega)$, $\boldsymbol{G}_{xy}(\omega)$, and ultimately $\boldsymbol{H}_{xy}(\omega)$.

In the experimental results reported in this work there were ten internal responses (as depicted in Fig. 2.2). Although an optimal set of internal response gages could have been found for the development of $\boldsymbol{H}_{xy}(\omega)$, all ten responses were used in the current research due to time constraints on the work conducted. Therefore, the transmissibility matrix was $10 \times 6 \times nfreq$, where *nfreq* is the number of discrete frequencies used for analysis. This paper presents $\boldsymbol{H}_{xy}(\omega)$ as a 2D matrix with the knowledge that it is solved at each frequency.

The first step in the verification process is assuring that the $\boldsymbol{H}_{xy}(\omega)$ matrix is of proper rank and well-conditioned. This is performed throughout each derivation method in this study. A large condition number is a good indicator of an ill-conditioned matrix. "As the condition number increases by a factor of ten; it is likely that one less digit of accuracy will be obtained in

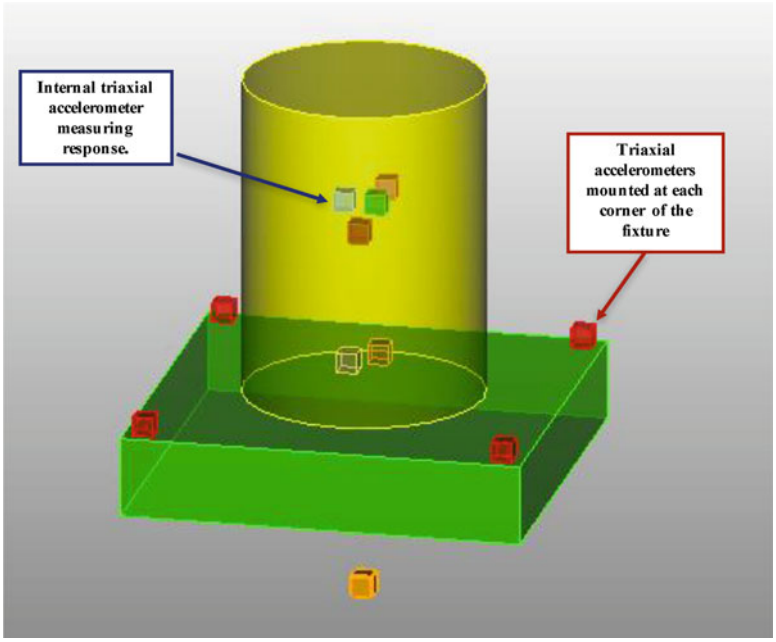

Fig. 2.2 Notional depiction of internal accelerometers

the solution" [7]. Generally, a double precision matrix provides 15 significant decimal digits [8]. Thus, a condition number of 1×10^{15} would indicate a singular matrix. In this study, any condition number below 5×10^{3} is considered appropriate.

2.3 Deriving the 6-DOF Shaker Table Input Given Flight Data

Once a transmissibility function is found for the test hardware (see Sect. 2.2), the various methods can be used to derive a 6-DOF input that is applicable for the test equipment. The 6-DOF input is in the form of an input spectral density matrix, denoted as $\boldsymbol{S}_{xx}(\omega)$, which is specified with coherence and phase for the off diagonal terms. It is imperative that $\boldsymbol{S}_{xx}(\omega)$ remain positive semidefinite, and checks are applied to assure this in each method. The four specific methods explored are discussed in the following subsections.

2.3.1 Method 1: PINV

The PINV method uses the typical input-output relation for linear systems, Eq. (2.1), but solving for the inputs as follows:

$$\boldsymbol{X}(\omega) = \left[\boldsymbol{H}_{xy}^{T}(\boldsymbol{\omega})\right]^{-\dagger} \boldsymbol{Y}_{\boldsymbol{flight}}(\omega), \tag{2.5}$$

where $\boldsymbol{Y}_{flight}(\omega)$ is the Fourier transforms of the acceleration responses from the field test data, $\boldsymbol{X}(\omega)$ is the Fourier transforms of the inputs, $\boldsymbol{a}_x$, and the superscript $[\ ]^T$ is the transpose of the matrix. The frequency spacing of $\boldsymbol{H}_{xy}(\omega)$ was interpolated to be the same as $\boldsymbol{Y}_{flight}(\omega)$, since $\boldsymbol{H}_{xy}(\omega)$ originally had a coarser frequency spacing. Once $\boldsymbol{X}(\omega)$ was found, it was used to calculate $\boldsymbol{S}_{xx}(\omega)$.

2.3.2 Method 2: ZINV

The input spectral density matrix can also be found from the following equation [5]:

$$\boldsymbol{S}_{xx}(\omega) = \boldsymbol{Z}_{xy}^{T*}(\omega)\, \boldsymbol{G}_{yy}(\omega)\, \boldsymbol{Z}_{xy}(\omega), \tag{2.6}$$

where $\boldsymbol{Z}_{xy}(\omega) = \boldsymbol{H}_{xy}^{-\dagger}(\omega)$, and the superscript $[\,]^{T^*}$ is the complex conjugate transpose. As was done with the previous method, the response spectral density matrix of the field data, $\boldsymbol{G}_{yy}(\omega)$, was interpolated to match frequency spacing of $\boldsymbol{H}_{xy}(\omega)$. As seen in the expression for the input spectral density matrix, this method also requires the inverse of the transmissibility function; however, for this particular approach two of such inverses are required.

2.3.3 Method 3: Scaling

This method explores the effect of scaling the results from Method 2: ZINV. Smallwood [4] developed a scaling method that assures the input matrix is positive semidefinite. In this study, all methods found a positive semidefinite input spectral density matrix; however, if straight-line specifications were developed from the inputs then scaling would be necessary. Therefore, scaling by Smallwood's method is explored to understand if there is any additional error introduced.

The scaling concept is done has follows. A new field response spectral density matrix is found by:

$$\boldsymbol{G}_{yy,scaled}(\omega) = \boldsymbol{S}_{\boldsymbol{s}}(\omega)\,\boldsymbol{G}_{yy}(\omega)\,\boldsymbol{S}_{s}(\omega)\,, \tag{2.7}$$

with

$$S_{s,ii}(\omega) = \sqrt{\frac{1}{G_{yy,ii}(\omega)}}, \tag{2.8}$$

where $\boldsymbol{S}_s(\omega)$ is the scaling matrix that only has values on the diagonals, $S_{s,ii}(\omega)$, that are found from the diagonal of the original response spectral density matrix of the field data, $\boldsymbol{G}_{yy}(\omega)$. Then a scaled input spectral density matrix, $\boldsymbol{S}_{xx,scaled}(\omega)$, can be found.

$$\boldsymbol{S}_{xx,scaled}(\omega) = \boldsymbol{Z}_{xy}^{T*}(\omega)\,\boldsymbol{G}_{yy,scaled}(\omega)\,\boldsymbol{Z}_{xy}(\omega)\,. \tag{2.9}$$

This now needs to be scaled back to obtain correct values, and this is accomplished as follows:

$$\boldsymbol{S}_{xx}(\omega) = \boldsymbol{Z}_{xy}^{T*}(\omega)\,\boldsymbol{S}_{s}^{-1}(\omega)\,\boldsymbol{H}_{xy}^{T*}(\omega)\,\boldsymbol{S}_{xx,scaled}(\omega)\,\boldsymbol{H}_{xy}(\omega)\,\boldsymbol{S}_{s}^{-1}(\omega)\,\boldsymbol{Z}_{xy}(\omega)\,. \tag{2.10}$$

2.3.4 Method 4: Smallwood–Cap

The final method explored in this work is a modified version of the one developed by Cap et al. [3]. This method has two interesting features. First, and most importantly, is the feature that it modifies the response spectral density matrix of the field data, $\boldsymbol{G}_{yy}(\omega)$, such that it does not use the off diagonal terms of the matrix, but it assures that the phase and coherence is compatible with the transmissibility matrix and through an iterative process the input spectral density matrix, $\boldsymbol{S}_{xx}(\omega)$. The second interesting feature is that it uses Tikhonov regularization. Tikhonov regularization is a simple and commonly used method for ill-posed problems.

Typical Tikhonov regularization for solving the equation $\boldsymbol{Ax} = \boldsymbol{b}$, is conducted by solving

$$\widehat{\boldsymbol{x}} = \left[\boldsymbol{A}^T\boldsymbol{A} - \lambda^2\boldsymbol{I}\right]^{-1}\boldsymbol{A}^T\boldsymbol{b}. \tag{2.11}$$

In this work, it is desired to solve $\boldsymbol{H}_{xy}^{T*}(\omega)\,\boldsymbol{S}_{xx}(\omega)\,\boldsymbol{H}_{xy}(\omega) = \boldsymbol{G}_{yy}(\omega)$ for $\boldsymbol{S}_{xx}(\omega)$. This is accomplished with Tikhonov regularization in a two-step process. First in the typical Tikhonov form, Eq. (2.11), set $\boldsymbol{A} = \boldsymbol{H}_{xy}^{T*}(\omega)\,, \boldsymbol{x} = \boldsymbol{S}_{xx}(\omega)\,\boldsymbol{H}_{xy}(\omega)$, and $\boldsymbol{b} = \boldsymbol{G}_{yy}(\omega)$, then solve for $\boldsymbol{S}_{xx}(\omega)\boldsymbol{H}_{xy}(\omega)$

$$\boldsymbol{S}_{xx}(\omega)\,\boldsymbol{H}_{xy}(\omega) = \left[\boldsymbol{H}_{xy}(\omega)\,\boldsymbol{H}_{xy}^{T*}(\omega) - \lambda^2\boldsymbol{I}\right]^{-1}\boldsymbol{H}_{xy}^{*}(\omega)\,\boldsymbol{G}_{yy}(\omega)\,. \tag{2.12}$$

For clarity assign the following:

$$\boldsymbol{D}(\omega) = \left[\boldsymbol{H}_{xy}^{*}(\omega)\boldsymbol{H}_{xy}^{T*}(\omega) - \lambda^2\boldsymbol{I}\right]^{-1}\boldsymbol{H}_{xy}^{*}(\omega)\boldsymbol{G}_{yy}(\omega). \tag{2.13}$$

Thus, Eq. (2.12) can be rewritten as follows:

$$\boldsymbol{S}_{xx}(\omega)\boldsymbol{H}_{xy}(\omega) = \boldsymbol{D}(\omega) \rightarrow \boldsymbol{H}_{xy}^{T*}(\omega)\boldsymbol{S}_{xx}^{T*}(\omega) = \boldsymbol{D}^{T*}(\omega). \tag{2.14}$$

Then the second step is another Tikhonov regularization on $\boldsymbol{H}_{xy}^{T*}(\omega)\boldsymbol{S}_{xx}^{T*}(\omega) = \boldsymbol{D}^{T*}(\omega)$, where $\boldsymbol{A} = \boldsymbol{H}_{xy}^{T}(\omega), \boldsymbol{x} = \boldsymbol{S}_{xx}^{T}(\omega)$, and $\boldsymbol{b} = \boldsymbol{D}^{T}(\omega)$.

$$\widehat{\boldsymbol{S}_{xx}^{T*}(\omega)} = \left[\boldsymbol{H}_{xy}(\omega)\boldsymbol{H}_{xy}^{T*}(\omega) - \lambda^2\boldsymbol{I}\right]^{-1}\boldsymbol{D}^{T*}(\omega). \tag{2.15}$$

Iterations can be performed setting $\boldsymbol{G}_{yy}(\omega) = \boldsymbol{H}_{xy}^{T*}(\omega)\widehat{\boldsymbol{S}_{xx}(\omega)}\boldsymbol{H}_{xy}(\omega)$.

During the Tikhonov regularization, the response spectral density matrix of the field data, $\boldsymbol{G}_{yy}(\omega)$ is modified to $\widehat{\boldsymbol{G}_{yy}(\omega)}$ as follows. First, the diagonals of the original $\boldsymbol{G}_{yy}(\omega)$ are copied: $\widehat{G_{yy,ii}(\omega)} = G_{yy,ii}(\omega)$. Next, the phase and coherence of $\widehat{\boldsymbol{G}_{yy}(\omega)}$ is set to be compatible with the transmissibility matrix, $\boldsymbol{H}_{xy}(\omega)$, and the input spectral density matrix, $\boldsymbol{S}_{xx}(\omega)$. This is done by first setting.

$$\boldsymbol{C}(\omega) = \boldsymbol{H}_{xy}^{T*}(\omega)\boldsymbol{S}_{xx}(\omega)\boldsymbol{H}_{xy}(\omega), \tag{2.16}$$

During the first iteration $\boldsymbol{S}_{xx}(\omega)$ is unknown and set to a diagonal matrix with 1×10^{-6} set on the diagonals. Now the off diagonals of $\boldsymbol{C}(\omega)$ are normalized as

$$C_{ijN}(\omega) = \frac{C_{ij}}{\sqrt{C_{ii}C_{jj}}}, \forall i \neq j. \tag{2.17}$$

Then, the off diagonals of $\widehat{G_{yy,ij}(\omega)} = C_{ijN}(\omega)$. Recall that the diagonal is the same as $\boldsymbol{G}_{yy}(\omega)$. Then, the off diagonals of $\widehat{G_{yy,ij}(\omega)}$ are scaled to values closer to $\boldsymbol{G}_{yy}(\omega)$ in the following manner

$$\widehat{G_{yy,ij}(\omega)} = C_{ijN}(\omega)\sqrt{G_{yy,ii}G_{yy,jj}}, \quad \forall i \neq j. \tag{2.18}$$

2.4 Comparison Metric for Methods

The ultimate assessment of the performance of each derivation method is given by a comparison of how well the methods reproduce the field data during the actual laboratory experiment. As mentioned, these results are presented in an accompanying paper to this work. However, two comparisons can be made at this time. The first is a comparison of the inputs to the field recommended input. However, this might be misleading as the field data is from a different unit. It is possible that these methods might correct for some unit-to-unit variability and the different boundary conditions found in flight and the laboratory. The second comparison is a prediction of the responses from each method.

Each method has a 6-DOF spectral density matrix (SDM) and a 3-DOF SDM. Including the rotational values adds some complexity; therefore, this study evaluated if just using translational (3-DOF) values would be appropriate.

2.4.1 Comparison of Inputs

The autospectral densities of the derived inputs are plotted in Figs. 2.3 and 2.4, for translational and rotational degrees of freedom respectively. It is difficult to make any firm recommendations on these values. It does appear that the 3-DOF predictions would put in less energy than the 6-DOF, because the translational ASD for the 3-DOF are generally of smaller magnitude.

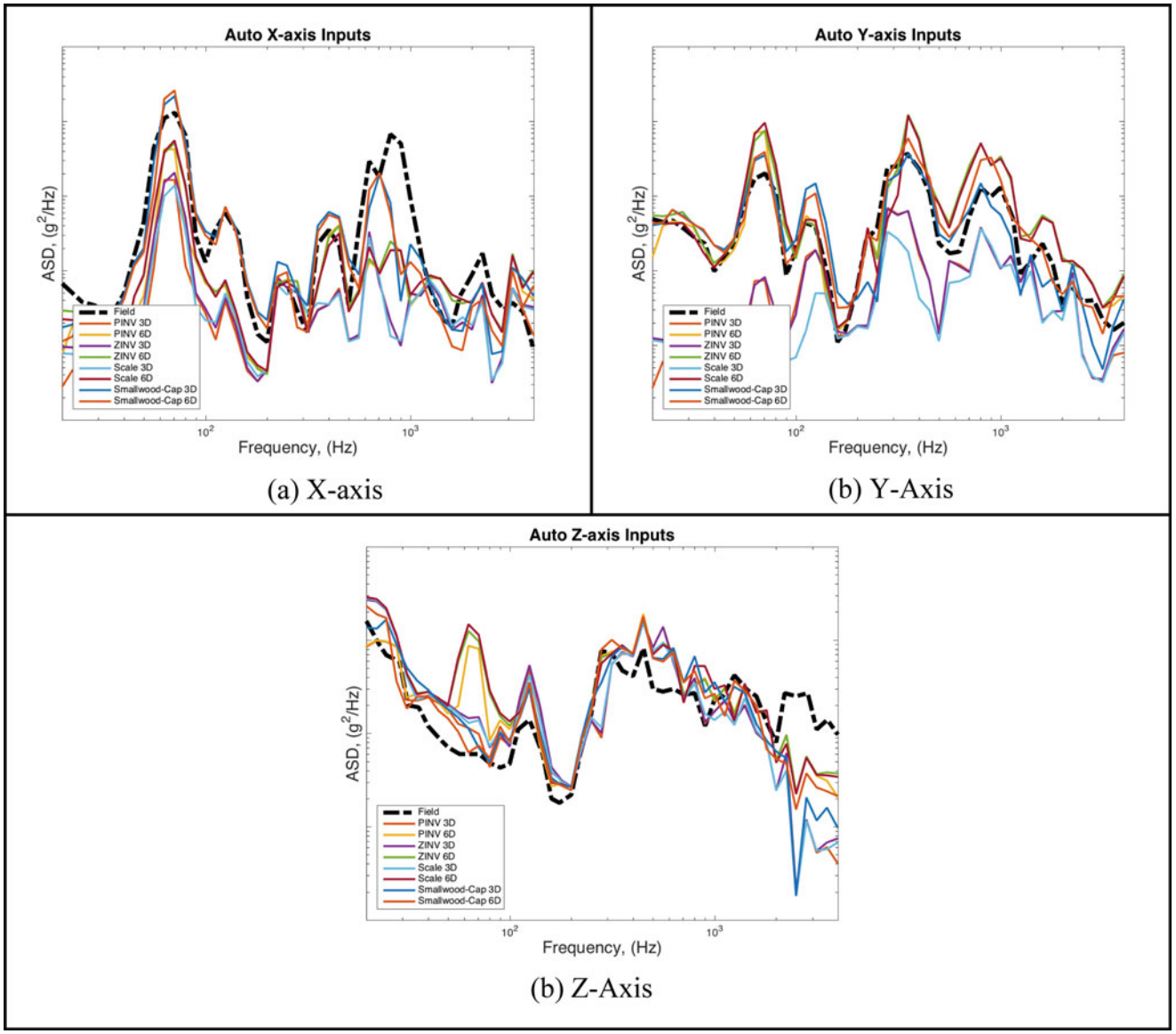

Fig. 2.3 Input comparisons of the different methods to the field data recommended input for translational values

2.4.2 Comparison of Predicted Responses to Actual Field Responses

Once the desired inputs are formed, the forward problem can be run numerically using the following equation from [9].

$$\boldsymbol{S}_{yy}(\omega) = \boldsymbol{H}_{xy}^{T*}(\omega)\,\boldsymbol{S}_{xx}(\omega)\,\boldsymbol{H}_{xy}(\omega)\,. \tag{2.19}$$

The predicted responses are denoted as $\boldsymbol{S}_{yy}(\omega)$ to keep a distinction from the actual response spectral density matrix of the field data, $\boldsymbol{G}_{yy}(\omega)$. This is of interest to see if, numerically, the desired input can be found such that $\boldsymbol{S}_{yy}(\omega)$ is a close approximation of $\boldsymbol{G}_{yy}(\omega)$. There will be some errors, since there are different units used for the field test as the one for the laboratory and that there are more internal gages as compared to inputs. In addition, there will be some numerical error associated with the interpolation done on several of the matrices.

In an effort to compare different methods, an error metric is established. First, the ASDs are filtered into 1/6th octave bands. Sixth octaves are chosen to attempt to accommodate any unit-to-unit variability. Then, an error in terms of decibels is found at each 1/6th octave frequency line, as follows:

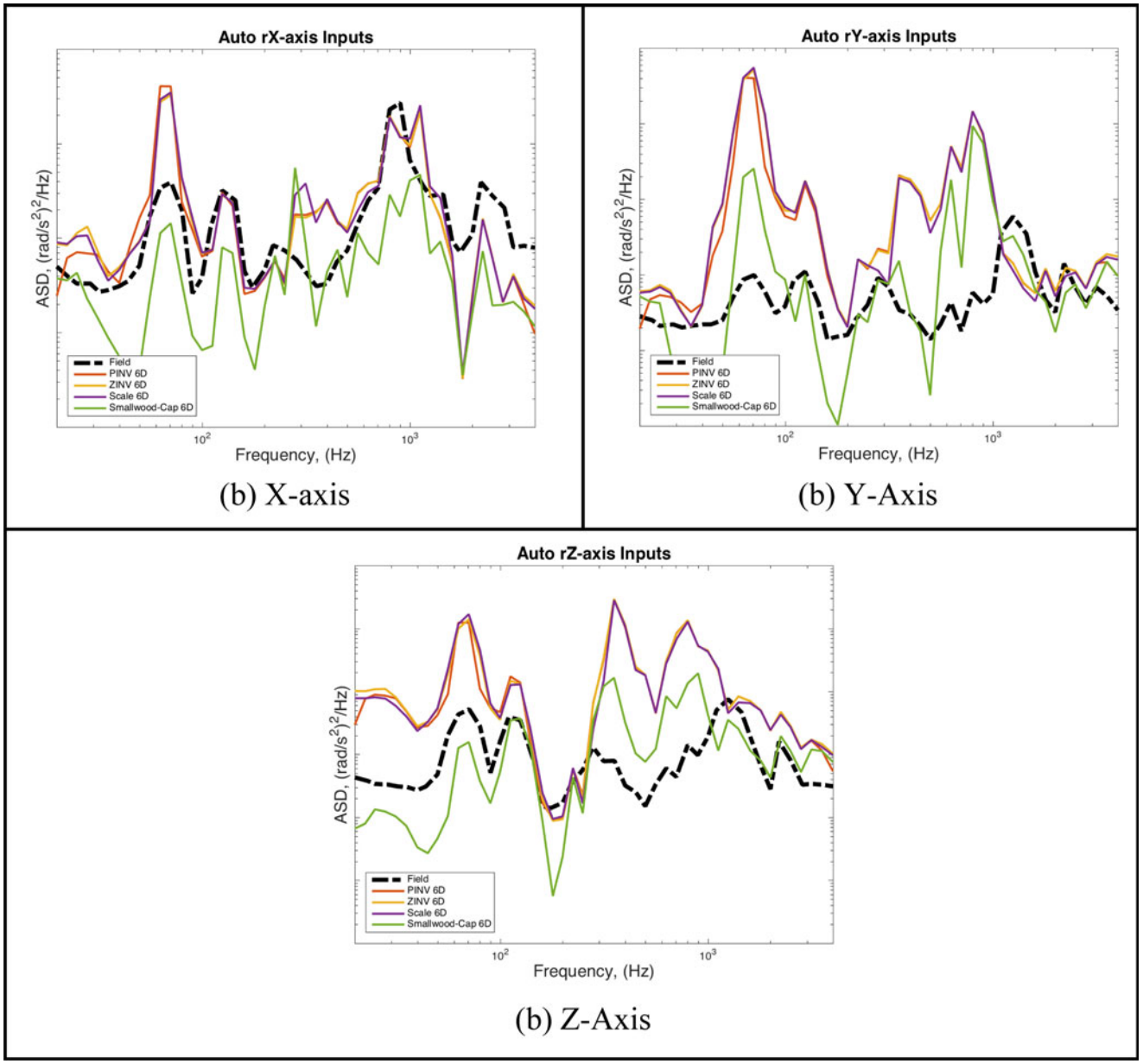

Fig. 2.4 Input comparisons of the different methods to the field data recommended input for rotational values

$$dB_{error}\left(\omega_{6th}\right) = 10 * log_{10} \frac{\boldsymbol{S}_{yy_{method}}\left(\omega_{6th}\right)}{\boldsymbol{G}_{yy}\left(\omega_{6th}\right)}. \tag{2.20}$$

Then, given the error at each frequency line in terms of decibels, three statistics can be generated for each method. The first is the statistics across each gage at each frequency line that is plotted as seen in Fig. 2.5. The second is the statistics across each gage, which is provided in Fig. 2.6. Finally, all error values at each frequency for each gage can be used to determine one mean and standard deviation for each method as seen in Fig. 2.7.

By comparing the predicted responses, some general trends have been noticed. First, the 3-DOF inputs appear to under excite the responses. Second, the Smallwood–Cap method appears to be the best method to choose, because it results in the smallest errors. Third, scaling appears to have very little effect when comparing the Scaling method to the ZINV method. This is useful information for when scaling is needed to keep the input spectral density matrix positive semidefinite.

Fig. 2.5 Error comparisons in terms of decibels at each frequency line for each method

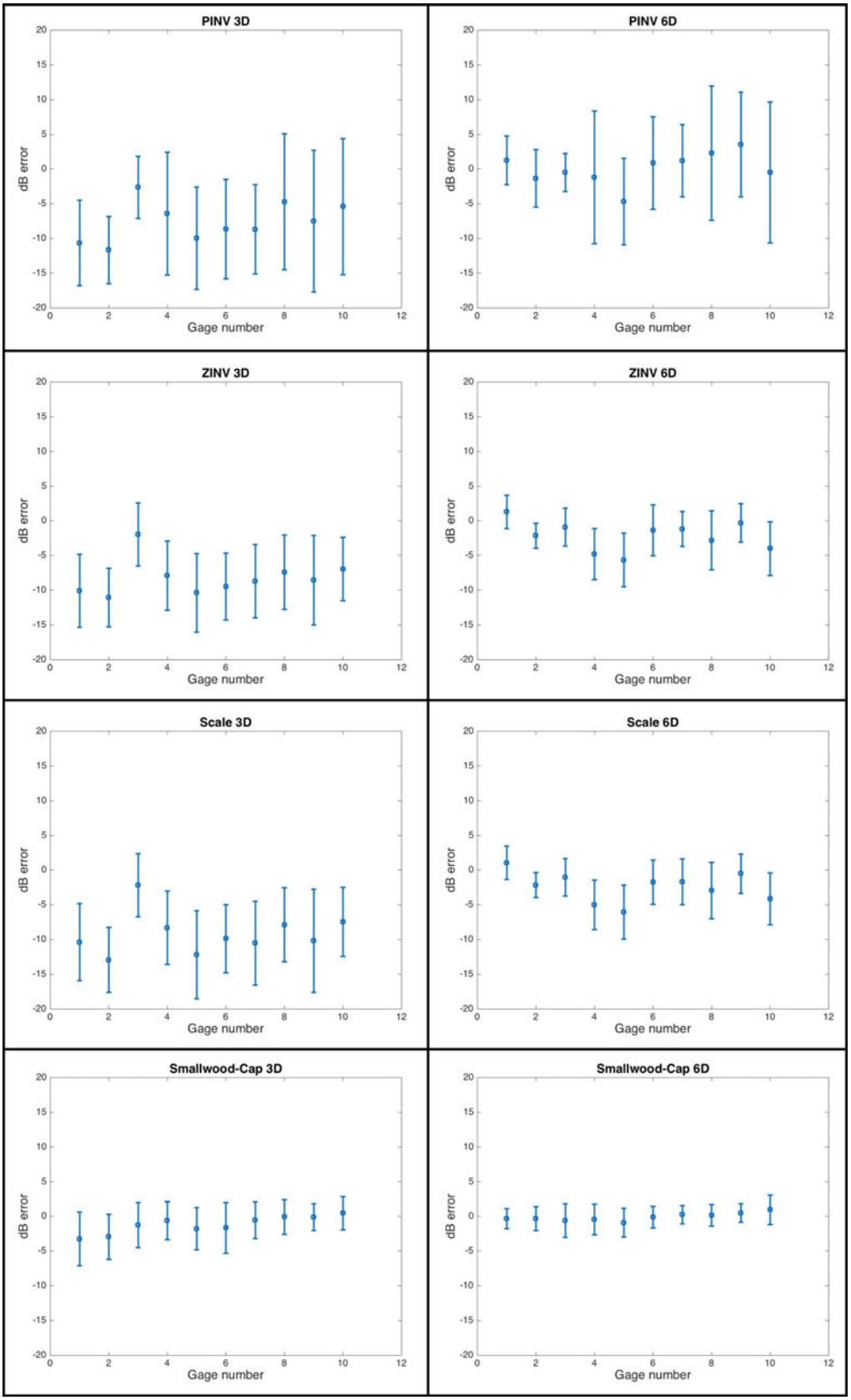

Fig. 2.6 Error comparisons in terms of decibels at each gage for each method

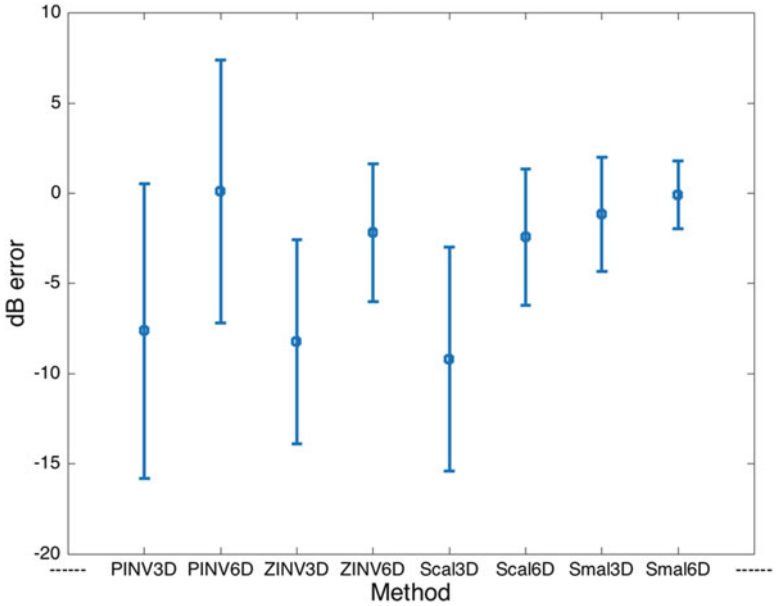

Fig. 2.7 Overall error comparisons among the different methods

2.5 Conclusions

This paper explores four different methods of deriving 6-DOF shaker inputs for a particular subsystem using an inverse methodology. An accompanying paper discusses the experimental set-up and the results of the actual experiment as compared to the flight data. This paper uses the transmissibility function and the recommended inputs to make predictions of the responses and compares those to the flight data. Each method explores using a full 6-DOF input of three translations and three rotations and only a 3-DOF input of just the translations. The predicted responses show that the 3-DOF input under excites the responses, that the Smallwood–Cap method produces the least amount of predicted error, and that scaling has very little effect on the error. Having little effect on the error is desirable for it has been shown that the input spectral density matrix may not be positive semidefinite, and scaling will correct this problem [4].

This work focused on potential methods to replicate an actual field test with a 6-DOF laboratory shaker test. Potential future work would include derivations of straight line specifications for the subsystem/component that is possible on the 6-DOF shaker. Also, the inverse problem could be proposed as an optimization problem and this might potentially derive the best input. Using an optimization algorithm could also have the benefit of assuring certain gages responses do not go below or above a certain amount, and gages could be given a weight to assure that they are met over others. Additional future work would be to explore the sources of error. It would be interesting to note if the inverse methods discussed correct for some of the errors.

Acknowledgements Sandia National Laboratories is a multi-mission laboratory managed and operated by Sandia Corporation, a wholly owned subsidiary of Lockheed Martin Corporation, for the U.S. Department of Energy's National Nuclear Security Administration under contract DE-AC04-94AL85000.

References

1. Tipton, D.G., Bitsie, F., Smallwood, D.O.: Comparison of the response of a simple structure to single axis and multiple axis random vibration inputs. In: 79th Shock Vibration Symposium, Orlando, 2008
2. Jacobs, L., Ross, M., Tipton, G., Cross, K., Hunter, N., Harvie, J., Nelson, G.: Experimental execution of 6DOF tests derived from field/flight tests. In: IMAC-XXXV Conference & Exposition on Structural Dynamics, Orange County, 2016
3. Cap, J., Tipton, D.G., Smallwood, D.O.: The derivation of random vibration specifications from field test data for use with a six degree-of-freedom shaker test. In: 80th Shock and Vibration Symposium, San Diego, October 2009
4. Smallwood, D.O.: A proposed method to generate a spectral density matrix for multiple input, multiple output (MIMO) vibration test. Shock. Vib. **14**(2), 107–132 (2007)

5. Bendat, J.S., Persol, A.G.: Random Data: Analysis and Measurement Procedures, 3rd edn. Wiley-Interscience Publication, New York (2000)
6. Owens, B., Tipton, D.G., McDowell, M.: 6 degree of freedom shock and vibration: testing and analysis. In: 86th shock and vibration symposium, Orlando, 2015
7. Atkinson, K.E.: An Introduction to Numerical Analysis, 2nd edn. John Wiley & Sons, New York (1988)
8. Kincaid, D., Cheney, W.: Numerical Analysis: Mathematics of Scientific Computing, 3rd edn. In: Pirtle, B. (ed.) Brooks/Cole (2002)
9. Wirsching, P.H., Paez, T.L., Ortiz, K.: Random Vibrations: Theory and Practice. Dover Publications, Inc., New York (1995)